

THE CONTRIBUTION OF HIGH REDSHIFT GALAXIES TO THE NEAR-INFRARED BACKGROUND

Bin Yue^{1,3,5}, Andrea Ferrara^{1,6}, Ruben Salvaterra², Xuelei Chen^{3,4}

ABSTRACT

Several independent measurements have confirmed the existence of a fluctuation excess ($\delta F_{\text{obs}} \approx 0.1 \text{ nW/m}^2/\text{sr}$ at $3.6 \mu\text{m}$) in the Near InfraRed Background (NIRB) up to degree angular scales, whose origin is unknown. By combining high resolution N-body/hydrodynamical cosmological simulations and an analytical model, we predict the absolute intensity and fluctuations impressed on the NIRB by high- z ($z > 5$) galaxies (some of which harboring Pop III stars, shown to provide a negligible contribution) and by simultaneously matching galaxy Luminosity Functions (LFs) and reionization constraints. This strategy also allows us to derive the phenomenological evolution of the ionizing photon escape fraction: we find $f_{\text{esc}} = 1$ at $z \geq 11$, decreasing to ≈ 0.05 at $z = 5$. In the wavelength range $1.0 - 4.5 \mu\text{m}$, the predicted cumulative NIRB flux is $F = 0.2 - 0.04 \text{ nW/m}^2/\text{sr}$. If galaxies brighter than $m_{\text{lim}} = 28$ can be removed, the remaining background from stellar sources will still contain a relevant contribution from galaxies at $z > 5$, showing that extraction of the reionization sources signal is feasible. However, we find that the radiation from high- z galaxies (including those undetected by current surveys) is insufficient to explain such excess: at $l = 2000$, the fluctuation strength is $\delta F = 0.01 - 0.002 \text{ nW/m}^2/\text{sr}$, with a relative amplitude $\delta F/F = 4\%$ almost independent of wavelength. Two problems remain unsolved: (a) both the predicted flux and fluctuations are considerably lower than the observed excess; (b) the fluctuation spectrum is redder (λ_0^p , with $p = -1.4$) than tentatively measured ($p = -3$). Both facts might indicate that an unknown component/foreground, with a clustering signal very similar to that of high- z galaxies, is dominating the NIRB radiation excess we receive on Earth.

Subject headings: cosmology—reionization—NIRB—high redshift galaxies

¹Scuola Normale Superiore, Piazza dei Cavalieri 7, I-56126 Pisa, Italy

²INAF, IASF Milano, via E. Bassini 15, I-20133 Milano, Italy

³National Astronomical Observatories, Chinese Academy of Sciences, 20A Datun Road, Chaoyang, Beijing 100012, China

⁴Center of High Energy Physics, Peking University, Beijing 100871, China

⁵Graduate University of Chinese Academy of Sciences, Beijing 100049, China

⁶Centennial B. Tinsley Professor, University of Texas, Austin, USA

1. INTRODUCTION

Observations of high redshift galaxies are essential to understand the reionization of the universe. The current surveys have reached redshifts $\sim 8-10$ (Bouwens et al. 2010, 2011a,b), however, it is generally believed that those detected sources, which are usually rare and bright galaxies, are not the dominant contributors to reionization (Choudhury & Ferrara 2007; Lorenzoni et al. 2011; Jaacks et al. 2012; Finkelstein et al. 2012), a large portion of galaxies being still below the detection limit. Furthermore, it is unlikely to find a substantial fraction of Pop III stars which are believed to start reionization in those detected galaxies, since usually they are old and have a long metal enrichment history (Salvaterra et al. 2011).

However, even without detecting galaxies individually, their cumulative flux has the potential to provide us key information on the reionization sources. Indeed, the bulk of their radiation emitted between the Lyman limit and the visible range, is redshifted into the near infrared band at present time. Therefore, the Near InfraRed Background (NIRB) residual, i.e., the remaining flux after removal of the contribution from our Solar system, from the Milky Way and the known foreground galaxies, would provide us a wealth of information of high redshift galaxies, such as their integrated emissivity and their large scale clustering properties, if it is really from those galaxies.

Measuring the NIRB has a history dating more than two decades (see the review by Kashlinsky 2005). Early measurements gave $\text{NIRB} > \sim 10 \text{ nW/m}^2/\text{sr}$ (Dwek & Arendt 1998; Gorjian et al. 2000; Matsumoto et al. 2000; Cambr sy et al. 2001; Matsumoto et al. 2005). It has already been confirmed that there indeed exist a non-zero excess when the foreground and the emission from the known galaxies in the field of view are removed, and this excess is hard to be attributed to the remaining known galaxy population below the detection limit (Totani et al. 2001; Matsumoto et al. 2005).

However, due to the difficulty in the foreground subtraction (Dwek et al. 2005), it is still hardly to accurately determine the absolute intensity, so more recent measurements pay more attention to intensity fluctuations, which can both exclude the influence of a strong but smooth foreground, i.e., the zodiacal light, and help to understand the large scale clustering properties of the sources (Kashlinsky et al. 2002; Magliocchetti et al. 2003; Cooray et al. 2004; Matsumoto et al. 2005; Salvaterra et al. 2006). The recent measurements (Kashlinsky et al. 2005, 2007a, 2012; Matsumoto et al. 2005, 2011; Thompson et al. 2007a,b) have obtained the angular power spectra of the NIRB residual at wavelengths from $1.1 \mu\text{m}$ to $8 \mu\text{m}$. Those power spectra show that the sources of the NIRB residual should have large angular scale clustering properties up to degree scales and indicate that the absolute intensity may be far smaller than previous measurements (for example, on arcmin scale the measured fluctuations amplitude is about $0.1 \text{ nW/m}^2/\text{sr}$ at wavelength $3.6 \mu\text{m}$; for relative fluctuations $\sim 10\%$, the absolute intensity should be only $\sim 1 \text{ nW/m}^2/\text{sr}$, see e.g. Arendt et al. 2010; Kashlinsky et al. 2012). Notably, Matsumoto et al. (2005) found that the intensity and fluctuation excess spectrum are both similar to a stellar spectrum, indicating that they might have the same origin.

Interpreting the above observations is fairly difficult. Salvaterra & Ferrara (2003) and Santos et al. (2002) suggested that Pop III stars could possibly be the sources of the residual excess. If true the NIRB would be an exquisite tool to study Pop III stars and high redshift galaxies. However, not long after Madau & Silk (2005) and Salvaterra & Ferrara (2006) found that this scenario needs a very high star formation efficiency, and may overpredict the high- z dropouts galaxies¹. On the other hand, Kashlinsky et al. (2005, 2007b); Matsumoto et al. (2011); Kashlinsky et al. (2012) still favor Pop III stars as the best candidate sources. Cooray et al. (2012) pointed out that models consistent with the optical depth of the free electrons after reionization measured by WMAP (Komatsu et al. 2011) predict much weaker fluctuation amplitude than observed (by about one order of magnitude). Numerical simulations by Fernandez et al. (2010, 2012) stressed the importance of the nonlinear effects in theoretical calculations to reconcile theory with data.

This is not the whole story, however. Some works (Thompson et al. 2007b; Cooray et al. 2007; Chary et al. 2008) proposed that lower redshift galaxies are possibly the sources of the observed fluctuations, but this possibility has become less attractive by now. Indeed, the recent work by Helgason et al. (2012) who reconstructed the emissivity history from the luminosity functions (LFs) of observed galaxies, found that fluctuations from the known galaxy population below the detection limit are unable to account for the observed clustering signal on sub-degree angular scales.

At least from a theoretical perspective, one key point is to predict more accurately the NIRB contributed by Pop III stars and galaxies before reionization, using models consistent with *all* the current observational constraints, e.g., including high redshift LFs and reionization. If the prediction matches the observational levels of both absolute intensity and fluctuations, we can go further and investigate in detail the contribution of Pop III stars and high redshift galaxies. If not, either our current theories about Pop III stars/high redshift galaxies must be revised, or we may need to find alternative explanations for the NIRB residual excess. To construct the star formation history from the birth of Pop III stars to the end of reionization as required to reliably predict the contribution to the NIRB, we should include the relevant physics of star/galaxy formation, e.g., gas dynamics, radiative cooling, supernova explosion and related metal production and transport, photoionization and heating, and the complex interactions among these processes.

In this paper, we attempt to make the most detailed theoretical NIRB modeling so far, enabling predictions of both the absolute intensity and angular power spectrum. We calculate the emissivity from simulations that include all the above physics, and especially a detailed treatment of chemical feedback (Tornatore et al. 2007a,b). The simulated LFs of high redshift galaxies match remarkably well the observations; this is the starting point of our NIRB model.

The layout of the paper is as follows. In Section 2 we introduce the simulation, and describe the steps to calculate the absolute intensity and the angular power spectrum. In Section 3 we

¹A significant contribution from high- z mini-quasars powered by accretion on to intermediate mass black holes with spectra similar to local Ultra-Luminous X-ray sources is disfavored on the basis of the unresolved X-ray background intensity constraints (Salvaterra et al. 2005).

present our results and compare them with observations. Conclusions are given in Section 4. In Appendix A we compare the different approximate solutions in the analytical calculation of the emissivity. Throughout this paper, we use the same cosmological parameters as in Salvaterra et al. (2011): $\Omega_m=0.26$, $\Omega_\Lambda=0.74$, $h=0.73$, $\Omega_b=0.041$, $n = 1$ and $\sigma_8=0.8$. The transfer function is from Eisenstein & Hu (1998). Magnitudes are in the AB system.

2. METHOD

2.1. The Absolute Intensity

At $z = 0$, the absolute intensity of the NIRB observed at frequency ν_0 is the integrated contribution of sources whose emission is shifted into a band of central frequency ν_0 . Following Salvaterra et al. (2006), we write it as

$$I_{\nu_0} = \int_{z_{\min}}^{z_{\max}} \epsilon(\nu, z) e^{-\tau_{\text{eff}}(\nu_0, z)} \frac{dr_p}{dz} dz = \int_{z_{\min}}^{z_{\max}} cdz \frac{\epsilon(\nu, z) e^{-\tau_{\text{eff}}(\nu_0, z)}}{H(z)(1+z)}, \quad (1)$$

where r_p is the proper distance, ν_0 is the frequency in the observer frame, $\nu = (1+z)\nu_0$ is the rest frame frequency, $\epsilon(\nu, z)$ is the comoving specific emissivity, $H(z) = H_0 \sqrt{\Omega_m(1+z)^3 + \Omega_\Lambda}$ is the Hubble parameter in a flat Λ CDM cosmology, c is the speed of light. The effective optical depth of absorbers between redshift 0 and z , τ_{eff} , is composed of two parts: the line absorption and the continuum absorption; we use the expressions in Salvaterra & Ferrara (2003).

We calculate the emissivity (see also Appendix for further discussion on subtleties related to the various approximations used in the literature) from the results of the simulations presented in Salvaterra et al. (2011), which include a detailed chemical enrichment treatment developed by Tornatore et al. (2007a). Both Pop II stars and Pop III stars are assumed to follow the Salpeter initial mass function (IMF) (Salpeter 1955), for Pop II stars the mass range is $0.1 - 100 M_\odot$, while for Pop III stars the mass range is $100 - 500 M_\odot$. Some recent works indicate that Pop III stars may not be as massive as several hundred Solar mass as predicted by previous theory, but may be limited to $\lesssim 50 M_\odot$ (Hosokawa et al. 2011). Our choice then corresponds to an upper limit to the contribution of these sources. Using those simulations, Salvaterra et al. (2011) generated the LFs of galaxies down to the magnitude far below the current observation limits at high redshifts. In the redshift range $5 < z < 10$, the simulated LFs match the observed ones almost perfectly in the overlapping luminosity range.

Suppose the specific luminosity of the i -th galaxy in the simulation box is $L_\nu^i(z)$ at redshift z , the comoving specific emissivity is

$$\epsilon(\nu, z) = \frac{1}{4\pi} \frac{\sum_{i=1}^N L_\nu^i(z)}{V}, \quad (2)$$

where V is the comoving volume of the simulation, N is the total number of galaxies in the simulation box at redshift z .

In the emissivity calculation, we must correct for rare bright galaxies that are not caught by the simulation due to the finite box size ($10 h^{-1}\text{Mpc}$). We follow the steps in Salvaterra et al. (2011). We first calculate the absolute magnitude corresponding to the mean luminosity of the two brightest galaxies in the simulation box, $M_{\text{UV,up}}$. The contribution (to be added to the numerator in Eq. (2)) from galaxies brighter than this magnitude is obtained by integration

$$L_{\nu}^{\text{corr}}(z) = V \int_{-25}^{M_{\text{UV,up}}} L_{\nu}^1(z) \frac{L_{\text{UV}}}{L_{\nu_{\text{UV}}}^1(z)} \Phi(M_{\text{UV}}, z) dM_{\text{UV}}, \quad (3)$$

where $L_{\nu}^1(z)$ is the luminosity of the brightest galaxy in the simulation (we assume all rare bright galaxies have the same Spectral Energy Distribution (SED) of this one), L_{UV} is the luminosity corresponding to the UV absolute magnitude M_{UV} . The wavelength used to calculate the absolute UV magnitude in this paper is 1700 \AA , ν_{UV} is the frequency corresponding to this wavelength. In observations, the selected wavelength corresponding to the UV absolute magnitude may be somewhat different in different measurements and at different redshifts (Bouwens et al. 2007; Oesch et al. 2010; Bouwens et al. 2010), however, our results are not sensitive to such differences. For the LF $\Phi(M_{\text{UV}}, z)$ in the redshift range $5 < z < 10$, we use the Schechter formula (Schechter 1976) with the redshift-dependent parameters given by Bouwens et al. (2011b) (see their Sec. 7.5), who fitted the observed LFs in $z \sim 4 - 8$ and extrapolate them to higher redshifts. For redshifts above 10, we simply add an exponential tail normalized to the simulated LF amplitude at $M_{\text{UV,up}}$. We find that the entire correction has only a small impact on our results. As discussed below (see also right panel of Figure 3), $\sim 90\%$ of the high- z galaxy contribution to the NIRB intensity comes from sources at $5 < z < 8$ where the correction is at most 12%. This correction is also applied to the calculation of ionizing photons below.

For each galaxy, the radiation comes from two different mechanisms: the stellar emission and the nebular emission. The former comes directly from the surface of stars, while the latter is generated by the ionized nebula around stars and depends on the fraction of ionizing photons that cannot escape into the intergalactic medium (IGM), i.e., $1 - f_{\text{esc}}$, where f_{esc} is the escape fraction. Ionizing photons escaping from galaxies would ionize the IGM; such ionized gas could also produce the nebular emission. However, due to the very low recombination rate, as shown in, e.g., Nakamoto et al. (2001) and Cooray et al. (2012), its emissivity is much weaker than the radiation from galaxies, so we ignore this contribution in this paper. The IGM contribution to the NIRB fluctuations is also negligible (Fernandez et al. 2010).

To determine the escape fraction averaged over the galaxy populations present at a given redshift, we proceed as follows. First we compute the number of ionizing photons emitted per baryon in collapsed objects as:

$$f_{\star} N_{\gamma} = \frac{1}{\sum_{i=1}^N M_{\text{gas}}^i} \sum_{i=1}^N \left[q_{\text{H}}^{\text{II}}(\tau^{\text{II},i}, Z^i) \dot{M}_{\star}^{\text{II},i} \tau^{\text{II},i} + q_{\text{H}}^{\text{III}} M_{\star}^{\text{III},i} \tau^{\text{III}} \right], \quad (4)$$

where q_{H}^{II} is the emission rate of ionizing photos from Pop II stars (this quantity depends on both the age and the metallicity of the stellar population) corresponding to a continuous star formation

rate $1 M_{\odot}\text{yr}^{-1}$. We derive this quantity from the Starburst99 templates² (Leitherer et al. 1999; Vázquez & Leitherer 2005; Leitherer et al. 2010) adopting the mean age, $\tau^{\text{II},i}$, and metallicity, Z^i , of each simulated galaxy. $q_{\text{H}}^{\text{III}}$ is the emission rate of ionizing photons for Pop III stars according to Schaerer (2002)³. M_{gas}^i is the gas content, $\dot{M}_{\star}^{\text{II},i}$ is the mean star formation rate of Pop II stars in this galaxy, while $M_{\star}^{\text{III},i}$ is the cumulative mass of Pop III stars. We use a mean lifetime $\tau^{\text{III}} = 2.5 \times 10^6$ yr for massive Pop III stars (Schaerer 2002; Salvaterra et al. 2011).

We then compare the above quantity with the number of ionizing photons per baryon in collapsed objects, N_{ion} , required by interpreting the observations as in Mitra et al. (2012a) (the “mean” value) to get the escape fraction, i.e., $f_{\text{esc}} = \min(\frac{CN_{\text{ion}}}{f_{\star}N_{\gamma}}, 1.0)$, where C is the clumping factor. Throughout this paper we assume $C = 1$ to get the minimum f_{esc} therefore the maximum contribution of the nebular emission to the NIRB. We note that the clumping factor could be higher than 1 even at high redshifts (Pawlik et al. 2009; Shull et al. 2012). For example, Shull et al. (2012) gives $C \approx 3$ (1.7) at $z = 5$ (9) by numerical simulations. Our nebular emission is therefore reduced by about 10% to 60% from $z = 5$ to $z = 9$ if this clumping factor is adopted. However, for Pop II stars which are the dominant contributors to the NIRB, the nebular emission is much smaller than the stellar emission. So the final reduction in the NIRB would be much smaller. Furthermore, we will show later that the flux from high redshift galaxies and Pop III stars is not able to explain the observed fluctuations level, so that a reduction in the NIRB intensity would in any case strengthen this conclusion. We plot the derived f_{esc} as a function of redshift in Figure 1. There is a clear trend of an increasing escape fraction towards higher redshifts; it reaches 1 at $z \approx 11$. At $z = 5$, the final redshift of the simulation, $f_{\text{esc}} \approx 0.05$. Although required by reionization data, an increasing trend of $f_{\text{esc}}(z)$ has not yet been fully understood theoretically in spite of the several, often conflicting, studies on this problem.

Based on observations, Inoue et al. (2006) concluded that $f_{\text{esc}} > 0.1$ when $z > 4$; by combining the observations of Lyman α absorption and UV LF, and also using N-body simulations and semi-analytical prescriptions to model the ionizing background, Srbínovsky & Wyithe (2010) found that for galaxies at $z \sim 5.5 - 6$, if the minimum mass of star forming galaxies corresponds to the hydrogen cooling threshold, $f_{\text{esc}} \sim 0.05 - 0.1$; Wyithe et al. (2010) used the star formation rate derived from gamma-ray burst observations to conclude that in the redshift range 4–8.5, $f_{\text{esc}} \sim 0.05$; Wise & Cen (2009), by radiation hydrodynamical simulations, found that at redshift 8 for galaxies with $M_{\text{vir}} < 10^{7.5} M_{\odot}$, $f_{\text{esc}} \sim 0.05 - 0.1$, while for more massive galaxies $f_{\text{esc}} \sim 0.4$, if a normal IMF is adopted; also via simulations, Razoumov & Sommer-Larsen (2010) found $f_{\text{esc}} \sim 0.8$ when $z = 10$. The escape fraction derived by us is broadly consistent with those values. The important difference however is that our derivation of f_{esc} matches both the LF and the reionization history simultaneously, i.e., a more phenomenological derivation. Different from our approach, Mitra et al.

²<http://www.stsci.edu/science/starburst99/docs/default.htm>

³Note the different dimensions of q_{H}^{II} and $q_{\text{H}}^{\text{III}}$: the former corresponds to per unit star formation rate while the latter corresponds to per unit stellar mass.

(2012b) computed the LFs of high redshift galaxies by means of semi-analytical models and derived the star formation efficiency f_* required to match the observed ones. They found $f_{\text{esc}} \approx 0.07$ at $z = 6$ and $f_{\text{esc}} \approx 0.16$ at $z = 7$, which are consistent with our $f_{\text{esc}} \approx 0.06$ (0.18) at those two redshifts. At higher redshifts, however, their escape fraction is somewhat lower than ours.

As a final remark, we underline that when computing the escape fraction, we do not make a distinction between Pop III and Pop II stars. Since in the calculation of $f_* N_\gamma$ we account for ionizing photons from both of them, one can think of f_{esc} as a kind of “effective” escape fraction averaged over the galaxy population. In principle, f_{esc} for Pop III stars should be higher due to their harder spectrum. However, as we will see in Section 3, Pop III stars only contribute a negligible flux to the present-day NIRB; a more detailed modeling is then not necessary.

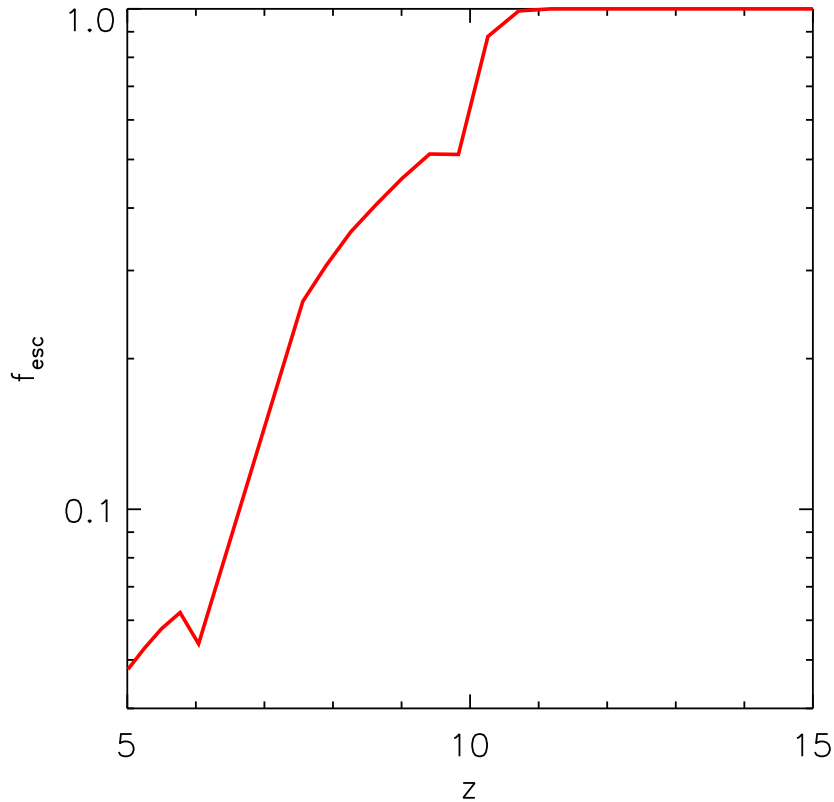


Fig. 1.— Escape fraction evolution from joint LF-reionization constraints.

The luminosity of the i -th galaxy, L_ν^i , is the sum of the contribution of Pop II and Pop III stars. For Pop II stars we use the age and metallicity dependent spectrum templates provided by the Starburst99 code. The nebular emission contribution has been renormalized by adopting

the escape fraction computed above. In addition to free-free, free-bound and two-photon emission which are already included in Starburst99, we add the Lyman α emission to the template by using (Fernandez & Komatsu 2006)

$$l_\alpha(\nu, \tau^{\text{II},i}, Z^i, z) = f_\alpha h_p \nu_\alpha \phi(\nu - \nu_\alpha) q_{\text{H}}^{\text{II}}(\tau^{\text{II},i}, Z^i) [1 - f_{\text{esc}}(z)], \quad (5)$$

in which $f_\alpha = 0.64$ (Fernandez & Komatsu 2006), h_p is the Plank constant, $\nu_\alpha = 2.47 \times 10^{15}$ Hz is the frequency of Lyman α photons. We use the line profile $\phi(\nu - \nu_\alpha)$ provided in Santos et al. (2002):

$$\phi(\nu - \nu_\alpha) = \begin{cases} \nu_\star(z)(\nu - \nu_\alpha)^2 \exp[-\nu_\star(z)/|\nu - \nu_\alpha|] & \text{when } \nu \leq \nu_\alpha \\ 0 & \text{when } \nu > \nu_\alpha, \end{cases} \quad (6)$$

where

$$\nu_\star(z) = 1.5 \times 10^{11} \left(\frac{\Omega_b h^2}{0.019} \right) \left(\frac{h}{0.7} \right)^{-1} \frac{(1+z)^3}{\sqrt{\Omega_m(1+z)^3 + \Omega_\Lambda}} \text{ Hz} \quad (7)$$

is the fitted form of results given in Loeb & Rybicki (1999).

For the template of Pop III stars, l_ν^{III} , we still use the spectrum in Schaerer (2002), but renormalize the nebular emission part by the factor $1 - f_{\text{esc}}$. The luminosity of the i -th galaxy is then (Salvaterra et al. 2011)

$$L_\nu^i(z) = l_\nu^{\text{II}}(\tau^{\text{II},i}, Z^i, z) \dot{M}_\star^{\text{II},i} + l_\nu^{\text{III}}(z) \dot{M}_\star^{\text{III},i} \tau^{\text{III}}, \quad (8)$$

the Lyman α emission in Eq. (5) is already included in l_ν^{II} here.

Given the above luminosity for each galaxy, we then get the emissivity according to Eq. (2). As an example, we plot the $\nu\epsilon(\nu, z)$ at redshift 12.0, 9.0 and 6.0 respectively in Figure 2. At high redshifts, the escape fraction is ≈ 1.0 , yielding a very weak Ly α line, since such emission is produced by recombinations of the ionized nebula around stars, which is ionized by the fraction $(1 - f_{\text{esc}})$ of the ionizing photons (dash-dotted line in Figure 2). At lower redshifts, due to a decreased escape fraction, the Ly α emission is clearly seen in the spectrum, as shown by the dashed and solid lines.

By focussing on the region of most interest here (energies below 10.2 eV), we find that spectrum becomes increasingly flatter with time. For example, at $z = 12$, the slope of $\nu\epsilon(\nu, z) \propto \nu^\beta$ with $\beta \approx 2$, while at $z = 5$ $\beta \approx 1.2$. This is clearly the result of an aging effect enhancing the rest frame optical/IR bands flux with respect to UV ones. Since the NIRB from $z > 5$ galaxies is dominated by lower redshift galaxies ($5 < z < 8$), we do not expect to get very steep NIRB spectra, as indeed we show in Sec. 3

2.2. NIRB Fluctuations

The angular power spectrum of the fluctuations of the specific intensity field given by Eq. (1) is (Cooray et al. 2012)

$$C_l^{\nu_0, \nu_0} = \int \frac{dz}{r^2(z)(1+z)^2} \frac{dr}{dz} [\epsilon(\nu, z) e^{-\tau_{\text{eff}}(\nu_0, z)}]^2 P_{\text{gg}}(k, z), \quad (9)$$

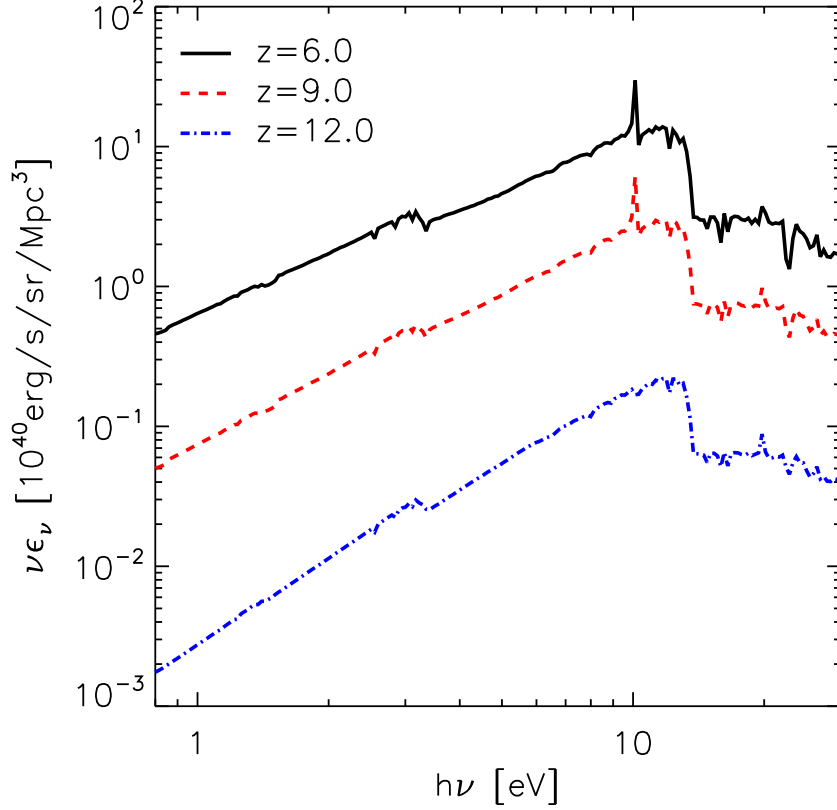


Fig. 2.— The emissivity of simulated galaxies at redshift 12.0 (dash-dotted), 9.0 (dashed) and 6.0 (solid) respectively.

where the comoving distance is $r(z) = \int_0^z \frac{cdz'}{H(z')}$, and $k = l/r(z)$. However, in observations what is really measured is the fluctuations of the “flux”, which is defined as $F = \nu_0 I_{\nu_0}$ (Kashlinsky 2005; Thompson et al. 2007a). To be consistent with this convention we replace $\epsilon(\nu, z)$ with $\nu_0 \epsilon(\nu, z) = \nu \epsilon(\nu, z)/(1+z)$, the above formula is then reduced to

$$C_l = \int_{z_{\min}}^{z_{\max}} cdz \frac{[\nu \epsilon(\nu, z) e^{-\tau_{\text{eff}}(\nu_0, z)}]^2}{H(z) r^2(z) (1+z)^4} P_{\text{gg}}(k, z); \quad (10)$$

without danger of confusion we ignore the superscript. Eq. (10) assumes that the luminous properties of galaxies are independent of their location, so the only factor that determines the fluctuations of the NIRB is their spatial fluctuations (see Shang et al. 2012 for an improved model), which is described by the galaxy-galaxy power spectrum, $P_{\text{gg}}(k, z)$.

The $10 h^{-1}$ Mpc box size of Salvaterra et al. (2011) simulations is too small to provide us with the large scale correlation function of galaxies (for sources at $z = 6$, the comoving trans-

verse separation corresponding to 1° angular size is about $100 h^{-1}\text{Mpc}$), so we use the halo model (Cooray & Sheth 2002; Cooray 2004) to calculate the galaxy-galaxy power spectrum. This power spectrum is composed of two parts, the one-halo term which means contributions from the correlation of galaxies (including the central galaxies and satellite galaxies) in the same halo, and the two-halo term from galaxies in different halos:

$$P_{\text{gg}}(k, z) = P_{\text{gg}}^{1h}(k, z) + P_{\text{gg}}^{2h}(k, z), \quad (11)$$

where, by assuming that the distribution of galaxies in a halo traces the profile of dark matter, and the mean number of central galaxies and satellite galaxies in a halo with mass M are $\langle N_{\text{sat}} \rangle$ and $\langle N_{\text{cen}} \rangle$, respectively,

$$P_{\text{gg}}^{1h}(k, z) = \int_{M_{\text{min}}(z)}^{M_{\text{max}}(z)} dM \frac{dn}{dM} \frac{2\langle N_{\text{sat}} \rangle \langle N_{\text{cen}} \rangle u(M, k) + \langle N_{\text{cen}} \rangle^2 u^2(M, k)}{\bar{n}_{\text{gal}}^2}, \quad (12)$$

and

$$P_{\text{gg}}^{2h}(k, z) = P_{\text{lin}}(k, z) \left[\int_{M_{\text{min}}(z)}^{M_{\text{max}}(z)} dM \frac{dn}{dM} b(M, z) \frac{\langle N_{\text{sat}} \rangle + \langle N_{\text{cen}} \rangle}{\bar{n}_{\text{gal}}} u(M, k) \right]^2. \quad (13)$$

In above expressions, $M_{\text{min}}(z)$ is the minimum mass of halos that could host galaxies, i.e., the minimum mass of halos that contribute to the emissivity. We set it to be the minimum mass of halos that contain stars in our simulations, which is $\sim (2 - 8) \times 10^7 M_\odot$, depending on redshift. $M_{\text{max}}(z)$ is the maximum mass contributing to the emissivity and the clustering (we describe how we determine it later on); dn/dM is the mass function (Sheth & Tormen 1999; Sheth et al. 2001), while $u(M, k)$ is the normalized Fourier transform of the halo profile. For a NFW profile (Navarro et al. 1997), the analytical expression is given by Cooray & Sheth (2002), and we use the concentration parameter, c_M , from Prada et al. (2012) which fits simulations well. However, we find that our results are insensitive to the use of different concentrations, as e.g., from Zehavi et al. (2011). Even if a concentration largely different from the above ones is adopted, its effects are non-negligible only in the one-halo term which dominates the signal at small scales, where galaxy clustering is well below the shot noise. Therefore, since we are mainly interested in the large-scale ($> 1'$) clustering, our conclusions are unaffected by the adopted value of c_M . Finally, $b(M, z)$ is the bias of halos relative to the dark matter; we use the formula given by Tinker et al. (2010) and the fitted parameters from simulations therein. This formula predicts higher bias for massive halos than Sheth et al. (2001), but is more close to simulations. The linear matter power spectrum, $P_{\text{lin}}(k, z)$, is from Eisenstein & Hu (1998).

The mean number of central galaxies and satellites in a halo with mass M is modeled by the halo occupation distribution (HOD) model (Zheng et al. 2005),

$$\langle N_{\text{cen}} \rangle = \frac{1}{2} \left[1 + \text{erf} \left(\frac{\log_{10} M - \log_{10} M_{\text{min}}}{\sigma_{\log_{10} M}} \right) \right], \quad (14)$$

and

$$\langle N_{\text{sat}} \rangle = \frac{1}{2} \left[1 + \text{erf} \left(\frac{\log_{10} M - \log_{10} 2M_{\text{min}}}{\sigma_{\log_{10} M}} \right) \right] \left(\frac{M}{M_{\text{sat}}} \right)^{\alpha_s}. \quad (15)$$

We adopt the parameters $M_{\text{sat}} = 15M_{\text{min}}$, $\sigma_{\log_{10}M} = 0.2$ and $\alpha_s = 1.0$, which are from both simulations and semi-analytical models (Zheng et al. 2005), and observations (Zehavi et al. 2011). With the mean number of central and satellite galaxies in each halo, the galaxy number density is simply

$$\bar{n}_{gal} = \int_{M_{\text{min}}(z)}^{M_{\text{max}}(z)} dM \frac{dn}{dM} (\langle N_{cen} \rangle + \langle N_{sat} \rangle). \quad (16)$$

In addition to the above galaxy clustering, Poisson fluctuations in the number of galaxies would generate shot noise in observations, whose power spectrum dominates at small scales. If the redshift derivative of the number of sources with flux between S and $S + dS$ is $\frac{d^2N}{dSdz}$, the angular power spectrum of such shot noise is

$$C_l^{\text{SN}} = \frac{1}{\Delta\Omega} \int dz \int dS S^2 \frac{d^2N}{dSdz} = \frac{1}{\Delta\Omega} \int dz \int dM S^2 \frac{d^2N}{dMdz}, \quad (17)$$

where $\Delta\Omega$ is the beam angle. Considering that

$$\frac{d^2N}{dMdz} = \frac{dn}{dM} \Delta\Omega r^2 \frac{dr}{dz}, \quad (18)$$

and

$$S = \frac{L_\nu(M) e^{-\tau_{\text{eff}}(\nu_0, z)}}{4\pi r^2 (1+z)}, \quad (19)$$

where $L_\nu(M)$ is the luminosity of halos with mass M , the shot noise power spectrum is

$$C_l^{\text{SN}} = \int dz \frac{e^{-\tau_{\text{eff}}(\nu_0, z)}}{r^2 (1+z)^2} \frac{dr}{dz} \int \left[\frac{L_\nu(M)}{4\pi M} \right]^2 M^2 \frac{dn}{dM} dM. \quad (20)$$

As we assume the luminous properties of galaxies are independent of their location, we can simply use an average light-to-mass ratio that is independent of halo mass,

$$\frac{L_\nu(M)}{4\pi M} = \int L_\nu(M) \frac{dn}{dM} dM \bigg/ 4\pi \int M \frac{dn}{dM} dM = \frac{\epsilon(\nu, z)}{\rho_h}. \quad (21)$$

As in the galaxy clustering, by replacing $\epsilon(\nu, z)$ with $\nu\epsilon(\nu, z)/(1+z)$, we finally get the shot noise angular power spectrum

$$C_l^{\text{SN}} = \int_{z_{\text{min}}}^{z_{\text{max}}} \frac{cdz}{H(z)r^2(z)(1+z)^4} P^{\text{SN}}(z), \quad (22)$$

where

$$P^{\text{SN}}(z) = \left[\frac{\nu\epsilon(\nu, z) e^{-\tau_{\text{eff}}}}{\rho_h} \right]^2 \int_{M_{\text{min}}(z)}^{M_{\text{max}}(z)} dM M^2 \frac{dn}{dM}, \quad (23)$$

and the halo mass density $\rho_h = \int_{M_{\text{min}}(z)}^{M_{\text{max}}(z)} dM M \frac{dn}{dM}$.

In observations, galaxies are generally removed down to a certain limiting magnitude, m_{lim} , to get the NIRB residual fluctuations. Thus, we need also to remove galaxies brighter than this limit

in the simulation box and in the bright-end. At $\lambda_0 = 1.6 \mu\text{m}$ Thompson et al. (2007a) adopted $m_{\text{lim}} \simeq 28$; at $\lambda_0 = 2.4 \mu\text{m}$ Matsumoto et al. (2011) reached $m_{\text{lim}} \simeq 23$; and at $\lambda_0 = 3.6, 4.5 \mu\text{m}$ Kashlinsky et al. (2012) used $m_{\text{lim}} \simeq 25$. The apparent limiting magnitude (at wavelength λ_0) is converted into the rest frame absolute magnitude (at wavelength $\lambda_0/(1+z)$) $M_{\lambda_0/(1+z)}$ by

$$M_{\lambda_0/(1+z)} = m_{\text{lim}} - DM(z) + 2.5\log_{10}(1+z), \quad (24)$$

where $DM(z)$ is the distance modulus (Helgason et al. 2012). By using a light-to-mass ratio constructed from the simulation, we determine the maximum halo mass $M_{\text{max}}(z)$ in the calculation of galaxy-galaxy power spectrum according to the above absolute magnitude. Things are slightly more complicated when calculating the absolute intensity and the spectrum of fluctuations, since they both depend on wavelength, while the limiting magnitude in observations at different wavelength is different. In this case we simply give the theoretical prediction without removing any sources in the simulation box and the bright-end, as shown by Figure 3 and Figure 7. We use $M_{\text{max}} = \infty$ and then we discuss the effects of galaxy removal, i.e., in Figure 4. Throughout this paper we adopt $z_{\text{min}} = 5$ and $z_{\text{max}} = 19$ unless otherwise specified.

3. RESULTS

We start by presenting the absolute intensity of the NIRB observed at $z = 0$ in the (observer frame) wavelength range $0.3 - 10 \mu\text{m}$ using Eq. (2) and the bright-end correction as defined by Eq. (3). Figure 3 (left panel) shows the predicted intensity $\nu_0 I_{\nu_0}$ (in cases without risk of confusion, we will refer to this variable as “flux”) when all sources with $z > 5$ are included; also shown separately are the contributions from Pop II and Pop III stars. The flux peak value is $0.2 \text{ nW/m}^2/\text{sr}$ at $\lambda_0 = 0.9 \mu\text{m}$, and decreases to $0.04 \text{ nW/m}^2/\text{sr}$ at $\lambda_0 = 4.5 \mu\text{m}$. The small bump on the left of the peak is due to intergalactic Ly α absorption by intervening neutral hydrogen.

We find that in our case, the Pop III contribution is almost negligible (it never exceeds 1%). This results from the fact that in the simulation the Pop III star formation rate is about three orders of magnitude lower than that of Pop II stars at $z = 10$; the ratio is even smaller below this redshift (Tornatore et al. 2007b). Stated differently, halos with the highest Pop III stellar fraction are usually smaller and less luminous, and their contribution to the total luminosity is very low (Salvaterra et al. 2011). So one should not be surprised that Pop III stars contribute negligibly to the NIRB. This prediction makes it more difficult to find Pop III signatures by means of NIRB observations.

In the right panel of Figure 3, we plot the contribution from sources above redshift 5.0, 8.0 and 12.0, respectively. It is clear that contributions from sources located at $5 < z < 8$ dominate, providing about 90% of the flux from all sources with $z > 5$. Most of those sources are the low-luminosity galaxies that cannot be detected individually in current surveys: they are believed to be the major contributors to reionization. In principle, then, the NIRB could be a perfect tool to study the reionization sources without detecting them individually.

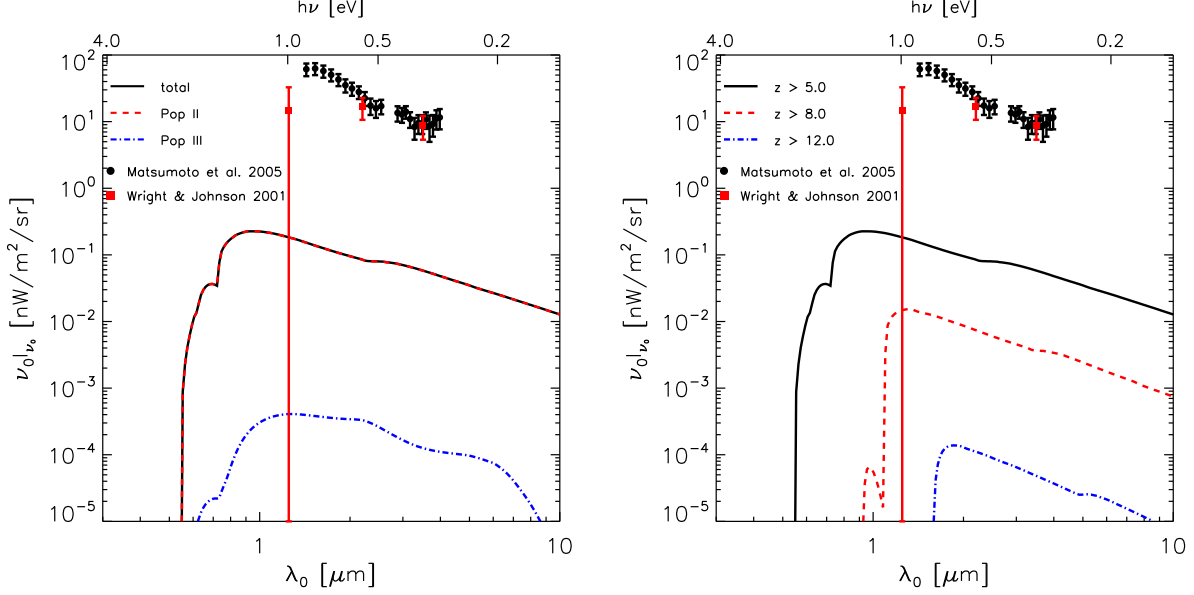


Fig. 3.— NIRB flux from high- z galaxies, $\nu_0 I_{\nu_0}$, at $z = 0$ as a function of wavelength in the observer frame. *Left panel:* Contributions from Pop II (dashed line), Pop III (dash-dotted) stars, and their sum. Since the contribution from Pop III stars is very small, the solid line and the dashed line are almost identical. *Right:* Contributions from sources in different redshift ranges: $z > 5$ (solid line), $z > 8$ (dashed) and $z > 12$ (dash-dotted). In both panels, circles (squares) refer to the measured isotropic emission by Matsumoto et al. (2005) (Wright & Johnson 2001) after subtraction of the contribution from galaxies with $z < 5$.

Using the LF constructed in Helgason et al. (2012), we calculate the integrated light of galaxies with $z < 5$. We then plot in Figure 3 the remaining flux after subtracting this component from the isotropic emission measured in Matsumoto et al. (2005) (circles) and Wright & Johnson (2001) (squares). Figure 3 clearly shows that even after such subtraction, the remaining flux in the measurements is $> 100\times$ larger than the theoretical prediction, indicating the need for another yet unknown component.

We plot the NIRB flux before and after removal of bright galaxies in Figure 4 at wavelengths from $1.25\ \mu\text{m}$ to $4.5\ \mu\text{m}$, corresponding to the band from J to M in Helgason et al. (2012). The crosses refer to flux from all galaxies with $z > 5$ in our work, while the solid line correspond to the flux from all galaxies in the default model of Helgason et al. (2012). After removal of galaxies brighter than $m_{\text{lim}} = 28$, the flux from $z > 5$ galaxies in our work is shown by diamonds, while flux from remaining galaxies in Helgason et al. (2012) is shown by the dashed line. The flux from all galaxies (solid line) is about 1-2 orders of magnitude larger than that from galaxies with $z > 5$ (crosses) in our work. Hence, without bright galaxy removal, $z < 5$ galaxies largely dominate the NIRB flux. However, if we remove the galaxies down to $m_{\text{lim}} = 28$, the flux from the remaining

galaxies at all redshifts in Helgason et al. (2012) (dashed line) is comparable to that from the remaining galaxies with $z > 5$ in our work. Even considering the uncertainties on the faint-end of LFs, in the source-subtracted flux, galaxies at $z > 5$ still contribute at least $\sim 20\%–30\%$. So we find that at least in principle we can indeed access the signal of reionization sources by subtracting the bright galaxies.

The fluctuations of the NIRB after subtracting galaxies down to the detection limits of observations, $\sqrt{l(l+1)C_l/(2\pi)}$, at $\lambda_0 = 1.6, 2.4, 3.6, 4.5 \mu\text{m}$ are shown by the thick solid line in each panel of Figure 5; the shot noise is also shown by a thick dashed line in each panel. At large scales, i.e., $l < 10^4$, the galaxy clustering is larger than the shot noise level, implying that $z > 5$ galaxies can indeed produce large scale clustering signatures. So the NIRB fluctuations do have the potential to provide us wealth of information of the clustering of the undetected reionization sources. However, compared with the observed values (shown by filled circles with errorbars) which are usually at $0.1 \text{ nW/m}^2/\text{sr}$ level (Thompson et al. 2007a; Matsumoto et al. 2011; Kashlinsky et al. 2012), our predictions are only $\sim (2-4) \times 10^{-3} \text{ nW/m}^2/\text{sr}$, i.e., much smaller than observations, indicating again the existence of unknown component(s) we are missing. Somewhat surprisingly (but interestingly) the missing component has a clustering signal very similar to that of high redshift galaxies and extending to degree angular scales. Obviously, this component/foreground should be removed before we are ready to exploit the NIRB to study reionization sources.

In each panel we also plot the galaxy clustering and the shot noise in the case without removal of galaxies by thin lines. Except for the $1.6 \mu\text{m}$ case in which galaxies are removed down to $m_{\text{lim}} = 28$, at different wavelengths the large scale galaxy clustering is almost unchanged, no matter whether the bright galaxies are removed or not. This implies that the corresponding limiting magnitude is not deep enough to see obvious changes of the galaxy clustering.

Next, we define $\delta F = \sqrt{l(l+1)C_l/(2\pi)}$ as the fluctuation amplitude and plot its ratio to $F = \nu_0 I_{\nu_0}$ in Figure 6. Such relative fluctuation is almost independent of the observed wavelength, λ_0 (see also Fernandez et al. 2010), and $\delta F/F \sim 4\%$ at $l = 2000$, with the only exception of the $1.6 \mu\text{m}$ band where it is somewhat lower than in redder bands, as a consequence of a deeper ($m_{\text{lim}} = 28$) galaxy removal. Nicely, the relative fluctuation agrees with that found by Fernandez et al. (2010) and Cooray et al. (2012). In addition, $\delta F/F$ increases with z_{min} , i.e., high redshift sources have higher relative fluctuations. For example, $\delta F/F = 7\%$ for $z_{\text{min}} = 8.0$, while it reaches 12% if $z_{\text{min}} = 12.0$ is adopted: although both δF and F decrease for larger z_{min} , the $k\sqrt{P_{\text{gg}}^{2h}(k, z)}$ term in δF reduces the decline rate of δF , since $k = l/r(z)$ corresponds to larger scales at higher redshifts if l is fixed. In other words, the higher is the redshift of the sources, the larger is the scale (and consequently P_{gg}^{2h}) contributing to the clustering signal. The relative fluctuation $\delta F/F$ is only weakly dependent on the intrinsic properties of galaxies (Fernandez et al. 2010), but more so on the spatial clustering features⁴. Thus, $\delta F/F$ is a key indicator to identify NIRB sources; yet, in

⁴As a sanity check, models that find a fluctuation level matching observations should avoid over-predicting the absolute intensity at the same time.

practice, it is hard to get an accurate absolute intensity.

The spectrum of the fluctuations, $\delta F(\lambda_0)$ from all galaxies with $z > 5$ at $l = 2000$, shown in Figure 7, has a slope λ_0^p , with $p = -1.4$ above $1 \mu\text{m}$. Such slope is essentially the same as that of the flux, reflecting the above mentioned wavelength independency of $\delta F/F$. There is circumstantial evidence from observations that the spectrum is instead “bluer” ($\sim \lambda_0^{-3}$, reminiscent of the Rayleigh-Jeans regime of a blackbody spectrum, e.g. Matsumoto et al. (2005, 2011)), or at least steeper than -1.4 . Our spectrum is redder basically for three reasons. First, the spectrum of a galaxy is the combination of spectra of stars spanning a wide mass range. Usually, it is redder than a typical massive star, unless a very top heavy IMF form is adopted. Second, galaxies close to the end of reionization ($z \sim 5 - 8$) contribute most to the integrated NIRB from high- z galaxies. Due to their larger ages and higher metallicity, those galaxies are usually redder than earlier systems. Third, Starburst99 includes not only the main sequence but also later evolutionary stages, during which stellar spectra become redder. The wavelength range $1.0 - 4.5 \mu\text{m}$ corresponds to a rest-frame energy $2 - 9 \text{ eV}$ provided the redshift of sources is ~ 6 . The slope of the fluctuation spectrum we predict is consistent with that of the flux spectrum around this redshift, i.e., the combination of the specific luminosity of galaxies with different ages, metallicity and so on in this energy range. If the data are confirmed, an important tension remains, as the blue colors in observations can hardly be attributed to the galaxy population consistent with the observed LFs and used in this paper to predict the NIRB.

4. CONCLUSIONS

By combining high resolution N-body/hydrodynamical cosmological simulations and an analytical model, we have predicted the absolute intensity and fluctuations impressed on the NIRB by high- z ($z > 5$) galaxies, some of which harboring Pop III stars. This is the most robust and detailed theoretical calculation done so far as we simultaneously match also the LFs and reionization constraints. The simulations include the relevant physics of galaxy formation and a novel treatment of chemical feedback, by following the metallicity evolution and implementing the physics of Pop III/Pop II transition based on a critical metallicity criterion. It is able to reproduce the observed UV LFs over the redshift range $5 < z < 10$, and extend it to faint magnitudes far below the detection limit of current observations.

We directly calculate the stellar emissivity from the simulations. We use Starburst99 to generate metallicity and age dependent SED templates, then calculate the luminosity for each galaxy according to its current star formation rate, stellar age and metallicity, instead of using a constant metallicity and average main sequence spectrum template. Except for the mass range of the IMF that has already been fixed in the simulation, there are no other free parameters in the calculation of the emissivity.

By comparing the number of ionizing photons produced per baryon in collapsed objects, $f_\star N_\gamma$,

in the simulation and the ionizing photon rate $N_{\text{ion}} \approx f_{\text{esc}} f_{\star} N_{\gamma}$ deduced from data-constrained reionization models, we get the evolution of the escape fraction of ionizing photons, $f_{\text{esc}}(z)$. We find $f_{\text{esc}} \approx 1$ at $z > 11$, decreasing to ≈ 0.05 at $z = 5$. This escape fraction is used to renormalize the nebular emission of Pop III and Pop II stars in the emissivity.

Pop III stars are unlikely to be responsible for the observed NIRB residual, as their contribution is very small ($< 1\%$) of the absolute intensity in our calculation. This is the natural result of the much lower star formation rate of Pop III stars compared with Pop II stars in the simulation, since even metals from a single Pop III star could enrich above the critical metallicity a large amount of gas around it (Tornatore et al. 2007b). The formation of Pop III stars is regulated by such a chemical feedback mechanism, which limits their contribution to the NIRB. However, a rapid Pop III-Pop II transition brings also a little advantage in terms of integrated emissivity, due to the longer lifetime of Pop II stars (Cooray et al. 2012).

We predict that in the wavelength range $1.0 - 4.5 \mu\text{m}$, the NIRB flux $F = \nu_0 I_{\nu_0} \sim 0.2 - 0.04 \text{ nW/m}^2/\text{sr}$, while the fluctuation strength is about $\delta F = 0.01 - 0.002 \text{ nW/m}^2/\text{sr}$ at $l = 2000$, when all $z > 5$ galaxies (and their Pop III stars) are accounted for. If we remove galaxies down to $m_{\text{lim}} = 28$, the above flux level is only slightly reduced; however, by comparing with Helgason et al. (2012), we find that the flux from $z < 5$ dramatically decreases and the remaining becomes comparable to the predicted signal. This implies that in principle it is possible to get the signal from reionization sources by subtracting galaxies down to a certain magnitude.

The relative fluctuation amplitude, $\delta F/F$, at $l = 2000$ is $\sim 4\%$, almost independently of the wavelength. This ratio may be helpful to investigate the clustering features of the NIRB sources, since the intrinsic properties of galaxies almost cancel out. Despite the difficulties in measuring the absolute intensity accurately, it could be treated as a quality indicator in the data reduction process: if a much higher/lower ratio is obtained from the data, this might suggest that a more careful analysis work is required to extract the genuine contribution from reionization sources.

In spite of being accurate and consistent with LFs and reionization data, thus offering a robust prediction of the NIRB contribution of high- z galaxies that likely reionized the universe, our interpretation leaves two open and puzzling questions.

First, both the predicted absolute flux and the fluctuations are considerably lower than observations, indicating that in addition to the contribution from the expected high- z galaxy population (and Pop III stars), we should invoke some other – yet unknown – missing component(s) or foreground(s) dominating the currently observed NIRB residual. The missing component has a clustering signal very similar to that of high redshift galaxies and extends to degree angular scales. Obviously, this component/foreground should be removed before we are ready to exploit the NIRB to study reionization sources. On the other hand, sources located at $5 < z < 8$ provide about 90% of the flux from all sources with $z > 5$ in our simulation; these are the faint galaxies currently undetected by deep surveys. Thus, if the above mentioned additional spurious sources/foregrounds can be removed reliably, the NIRB will become the primary tool to investigate the properties of

the reionizing sources.

Second, the fluctuation spectrum is redder/flatter (λ_0^p , with $p = -1.4$) than that suggested by the data, which seems to favor a slope close to a black body spectrum in the Rayleigh-Jeans regime ($p = -3$). In principle this could only be explained in the rather unlikely case in which the spectrum is dominated by massive Pop III stars with a very peaked IMF⁵. Our study and related ones (Maio et al. 2010; Wise et al. 2012) however strongly disfavor such an extreme scenario. As “normal” galaxies observed in the HUDF tend to have SEDs consistent with our predictions, the blue color of the spectrum, if confirmed, might again point towards the fact that an unknown component/foreground is dominating the residual NIRB radiation we receive on Earth.

ACKNOWLEDGMENTS

It is a pleasure to acknowledge intense discussions and data exchange with A. Cooray, K. Helgason, E. Komatsu, T. Matsumoto, R. Thompson, S. Kashlinsky, S. Mitra and T. Choudhury. AF thanks UT Austin for support and hospitality as a Centennial B. Tinsley Professor and the stimulating atmosphere of the NIRB Workshop organized by the Texas Cosmology Center.

REFERENCES

- Arendt, R. G., Kashlinsky, A., Moseley, S. H., & Mather, J. 2010, *ApJS*, 186, 10
- Bouwens, R. J., Illingworth, G. D., Franx, M., & Ford, H. 2007, *ApJ*, 670, 928
- Bouwens, R. J. et al. 2011a, *Nature*, 469, 504
- . 2011b, *ApJ*, 737, 90
- . 2010, *ApJ*, 709, L133
- Cambr  sy, L., Reach, W. T., Beichman, C. A., & Jarrett, T. H. 2001, *ApJ*, 555, 563
- Chary, R.-R., Cooray, A., & Sullivan, I. 2008, *ApJ*, 681, 53
- Choudhury, T. R., & Ferrara, A. 2007, *MNRAS*, 380, L6
- Cooray, A. 2004, *MNRAS*, 348, 250
- Cooray, A., Bock, J. J., Keatin, B., Lange, A. E., & Matsumoto, T. 2004, *ApJ*, 606, 611
- Cooray, A., Gong, Y., Smidt, J., & Santos, M. G. 2012, *ArXiv e-prints*, 1205.2316

⁵In this extreme scenario we should further require $f_{\text{esc}} \sim 1$ to avoid a large contribution of the nebular emission.

- Cooray, A., & Sheth, R. 2002, *Phys. Rep.*, 372, 1
- Cooray, A. et al. 2007, *ApJ*, 659, L91
- Dwek, E., & Arendt, R. G. 1998, *ApJ*, 508, L9
- Dwek, E., Arendt, R. G., & Krennrich, F. 2005, *ApJ*, 635, 784
- Eisenstein, D. J., & Hu, W. 1998, *ApJ*, 496, 605
- Fernandez, E. R., Iliev, I. T., Komatsu, E., & Shapiro, P. R. 2012, *ApJ*, 750, 20
- Fernandez, E. R., & Komatsu, E. 2006, *ApJ*, 646, 703
- Fernandez, E. R., Komatsu, E., Iliev, I. T., & Shapiro, P. R. 2010, *ApJ*, 710, 1089
- Finkelstein, S. L. et al. 2012, *ArXiv e-prints*, 1206.0735
- Girardi, L., Bressan, A., Bertelli, G., & Chiosi, C. 2000, *A&AS*, 141, 371
- Gorjian, V., Wright, E. L., & Chary, R. R. 2000, *ApJ*, 536, 550
- Helgason, K., Ricotti, M., & Kashlinsky, A. 2012, *ApJ*, 752, 113
- Hosokawa, T., Omukai, K., Yoshida, N., & Yorke, H. W. 2011, *Science*, 334, 1250
- Inoue, A. K., Iwata, I., & Deharveng, J.-M. 2006, *MNRAS*, 371, L1
- Jaacks, J., Choi, J.-H., Nagamine, K., Thompson, R., & Varghese, S. 2012, *MNRAS*, 420, 1606
- Kashlinsky, A. 2005, *Phys. Rep.*, 409, 361
- Kashlinsky, A., Arendt, R. G., Ashby, M. L. N., Fazio, G. G., Mather, J., & Moseley, S. H. 2012, *ApJ*, 753, 63
- Kashlinsky, A., Arendt, R. G., Mather, J., & Moseley, S. H. 2005, *Nature*, 438, 45
- . 2007a, *ApJ*, 654, L5
- . 2007b, *ApJ*, 654, L1
- Kashlinsky, A., Odenwald, S., Mather, J., Skrutskie, M. F., & Cutri, R. M. 2002, *ApJ*, 579, L53
- Komatsu, E. et al. 2011, *ApJS*, 192, 18
- Leitherer, C., Ortiz Otálvaro, P. A., Bresolin, F., Kudritzki, R.-P., Lo Faro, B., Pauldrach, A. W. A., Pettini, M., & Rix, S. A. 2010, *ApJS*, 189, 309
- Leitherer, C. et al. 1999, *ApJS*, 123, 3

- Loeb, A., & Rybicki, G. B. 1999, *ApJ*, 524, 527
- Lorenzoni, S., Bunker, A. J., Wilkins, S. M., Stanway, E. R., Jarvis, M. J., & Caruana, J. 2011, *MNRAS*, 414, 1455
- Madau, P., & Silk, J. 2005, *MNRAS*, 359, L37
- Magliocchetti, M., Salvaterra, R., & Ferrara, A. 2003, *MNRAS*, 342, L25
- Maio, U., Ciardi, B., Dolag, K., Tornatore, L., & Khochfar, S. 2010, *MNRAS*, 407, 1003
- Matsumoto, T. et al. 2000, in *Lecture Notes in Physics*, Berlin Springer Verlag, Vol. 548, *ISO Survey of a Dusty Universe*, ed. D. Lemke, M. Stickel, & K. Wilke, 96
- Matsumoto, T. et al. 2005, *ApJ*, 626, 31
- . 2011, *ApJ*, 742, 124
- Mitra, S., Choudhury, T. R., & Ferrara, A. 2012a, *MNRAS*, 419, 1480
- Mitra, S., Ferrara, A., & Choudhury, T. R. 2012b, *ArXiv e-prints*, 1207.3803
- Nakamoto, T., Umemura, M., & Susa, H. 2001, *MNRAS*, 321, 593
- Navarro, J. F., Frenk, C. S., & White, S. D. M. 1997, *ApJ*, 490, 493
- Oesch, P. A. et al. 2010, *ApJ*, 709, L16
- Pawlik, A. H., Schaye, J., & van Scherpenzeel, E. 2009, *MNRAS*, 394, 1812
- Prada, F., Klypin, A. A., Cuesta, A. J., Betancort-Rijo, J. E., & Primack, J. 2012, *MNRAS*, 423, 3018
- Razoumov, A. O., & Sommer-Larsen, J. 2010, *ApJ*, 710, 1239
- Salpeter, E. E. 1955, *ApJ*, 121, 161
- Salvaterra, R., & Ferrara, A. 2003, *MNRAS*, 339, 973
- . 2006, *MNRAS*, 367, L11
- Salvaterra, R., Ferrara, A., & Dayal, P. 2011, *MNRAS*, 414, 847
- Salvaterra, R., Haardt, F., & Ferrara, A. 2005, *MNRAS*, 362, L50
- Salvaterra, R., Magliocchetti, M., Ferrara, A., & Schneider, R. 2006, *MNRAS*, 368, L6
- Santos, M. R., Bromm, V., & Kamionkowski, M. 2002, *MNRAS*, 336, 1082
- Schaerer, D. 2002, *A&A*, 382, 28

- Schechter, P. 1976, *ApJ*, 203, 297
- Shang, C., Haiman, Z., Knox, L., & Oh, S. P. 2012, *MNRAS*, 421, 2832
- Sheth, R. K., Mo, H. J., & Tormen, G. 2001, *MNRAS*, 323, 1
- Sheth, R. K., & Tormen, G. 1999, *MNRAS*, 308, 119
- Shull, J. M., Harness, A., Trenti, M., & Smith, B. D. 2012, *ApJ*, 747, 100
- Srbinovsky, J. A., & Wyithe, J. S. B. 2010, *PASA*, 27, 110
- Thompson, R. I., Eisenstein, D., Fan, X., Rieke, M., & Kennicutt, R. C. 2007a, *ApJ*, 657, 669
- . 2007b, *ApJ*, 666, 658
- Tinker, J. L., Robertson, B. E., Kravtsov, A. V., Klypin, A., Warren, M. S., Yepes, G., & Gottlöber, S. 2010, *ApJ*, 724, 878
- Tornatore, L., Borgani, S., Dolag, K., & Matteucci, F. 2007a, *MNRAS*, 382, 1050
- Tornatore, L., Ferrara, A., & Schneider, R. 2007b, *MNRAS*, 382, 945
- Totani, T., Yoshii, Y., Iwamuro, F., Maihara, T., & Motohara, K. 2001, *ApJ*, 550, L137
- Vázquez, G. A., & Leitherer, C. 2005, *ApJ*, 621, 695
- Wise, J. H., & Cen, R. 2009, *ApJ*, 693, 984
- Wise, J. H., Turk, M. J., Norman, M. L., & Abel, T. 2012, *ApJ*, 745, 50
- Wright, E. L., & Johnson, B. D. 2001, *ArXiv Astrophysics e-prints*, arXiv:astro-ph/0107205
- Wyithe, J. S. B., Hopkins, A. M., Kistler, M. D., Yüksel, H., & Beacom, J. F. 2010, *MNRAS*, 401, 2561
- Zehavi, I. et al. 2011, *ApJ*, 736, 59
- Zheng, Z. et al. 2005, *ApJ*, 633, 791

A. AN ANALYTICAL DERIVATION OF THE EMISSIVITY

At redshift z , the emissivity (defined as energy emitted per unit comoving volume per unit frequency per unit steradian here) of stellar population at frequency ν is given by the following integral (Fernandez & Komatsu 2006):

$$\epsilon(\nu, z) = \frac{1}{4\pi} \int_{m_1}^{m_2} L_\nu(m) n_\star(m) dm, \quad (\text{A1})$$

where $L_\nu(m)$ is the specific luminosity of a star with mass m , m_1 is the minimum mass of stars while m_2 is the maximum mass, $n_\star(m)$ is the number density of *alive* stars between m and $m + dm$, which is written as

$$n_\star(m) = \int_{t(z)-\tau(m)}^{t(z)} \dot{n}_\star(m, t') dt', \quad (\text{A2})$$

where $t(z)$ is the age of the universe at redshift z , $\tau(m)$ is the lifetime of a star with mass m . For Pop II stars with metallicity $1/50 Z_\odot$, useful fitting formulae for these quantities as a function of m are collected in Fernandez & Komatsu (2006). Eq. (A2) means that only stars formed between $t(z) - \tau(m)$ and $t(z)$ can still emit photons at time $t(z)$. The formation rate of stars with mass between m and $m + dm$, $\dot{n}_\star(m, t')$, is

$$\dot{n}_\star(m, t') = \frac{\dot{\rho}_\star(t')}{m_\star} f(m), \quad (\text{A3})$$

in which $f(m)$ is the normalized stellar IMF, i.e., $\int_{m_1}^{m_2} f(m) dm = 1$ and $m_\star = \int_{m_1}^{m_2} m f(m) dm$, while

$$\dot{\rho}_\star(t') = f_\star \frac{\Omega_b}{\Omega_m} \int_{M_{\min}}^{\infty} M \frac{d^2 n}{dM dt'}(M, t') dM \quad (\text{A4})$$

is the comoving star formation rate density in halos above mass M_{\min} , provided a fraction f_\star of baryons are converted into stars.

Two approximate solutions can be found under particular circumstances. If the star formation rate is almost constant over the time interval $\tau(m)$, i.e., $\tau(m) < t_{\text{SF}}(z)$, where the star formation time scale $t_{\text{SF}}(z) = \left[\frac{\dot{\rho}_\star(z)}{\rho_\star} \right]^{-1}$, then

$$\int_{t(z)-\tau(m)}^{t(z)} \dot{\rho}_\star(t') dt' \approx \dot{\rho}_\star[t(z)] \tau(m),$$

and the emissivity is approximated as (Fernandez & Komatsu 2006; Fernandez et al. 2010)

$$\epsilon(\nu, z) = \frac{1}{4\pi} \frac{\dot{\rho}_\star(z)}{m_\star} \int_{m_1}^{m_2} L_\nu(m) \tau(m) f(m) dm, \quad (\text{A5})$$

which is usually used for relative massive stars with short lifetime, we name it ‘‘Approximation 1’’.

On the other hand, if $\tau(m)$ is longer than the age of the universe (this is true for stars of smaller mass, and means that no stars die),

$$\int_{t(z)-\tau(m)}^{t(z)} \frac{\dot{\rho}_*(t')}{m_*} dt' = \int_0^{t(z)} \frac{\dot{\rho}_*(t')}{m_*} dt' = \frac{\rho_*(z)}{m_*}, \quad (\text{A6})$$

the emissivity becomes (Fernandez & Komatsu 2006)

$$\epsilon(\nu, z) = \frac{1}{4\pi} \frac{\rho_*(z)}{m_*} \int_{m_1}^{m_2} L_\nu(m) f(m) dm. \quad (\text{A7})$$

This also holds true if $\tau(m)$ is much longer than the star formation time scale $t_{\text{SF}}(z)$, i.e. the death of stars is less significant compared with the formation of new stars, so that

$$\int_{t(z)-\tau(m)}^{t(z)} \frac{\dot{\rho}_*(t')}{m_*} dt' = \frac{\Delta\rho_*(z)}{m_*} \approx \frac{\rho_*(z)}{m_*}, \quad (\text{A8})$$

and the emissivity could also be approximated as Eq. (A7), and we call it “Approximation 2”.

In reality, a galaxy is composed of stars with different mass; some of them may have lifetime longer than t_{SF} , while others not. In this case a “Hybrid” approximation could be used,

$$\epsilon(\nu, z) = \frac{1}{4\pi} \left[\frac{\rho_*(z)}{m_*} \int_{m_1}^{m_t} L_\nu(m) f(m) dm + \frac{\dot{\rho}_*(z)}{m_*} \int_{m_t}^{m_2} L_\nu(m) \tau(m) f(m) dm \right], \quad (\text{A9})$$

where m_t is the stellar mass determined by the condition $\tau(m_t) = t_{\text{SF}}$.

We compare the full analytical solution of Eqs. (A1-A4) with these three approximate solutions. Furthermore, we will also consider the emissivity obtained by adopting the Starburst99 template at $Z = 1/50 Z_\odot$ instead of the simplified fitting formula by Fernandez & Komatsu (2006). In this case the emissivity is given by

$$\epsilon(\nu, z) = \frac{1}{4\pi} \int_0^{t(z)} L_{\nu, \text{SB99}}[z, t(z) - t'] \dot{\rho}_*(t') dt', \quad (\text{A10})$$

where $L_{\nu, \text{SB99}}$ is the luminosity per unit mass (note that here for integration purposes we use the burst star formation model) from Starburst99.

In our work, the mass range of Pop II stars is $0.1 - 100 M_\odot$, while the fitted formula of the main sequence age used in Fernandez & Komatsu (2006), Fernandez et al. (2010) and Cooray et al. (2012) (taken from Schaerer 2002) is based on data of massive stars. To avoid introducing more uncertainties, in this comparison we adopt a mass range $1 - 100 M_\odot$ for Pop II stars. We checked that for Pop II stars with mass $1 M_\odot$, the fitted main sequence age still agrees with Girardi et al. (2000).

Since Pop II stars are found to contribute much more than Pop III stars to the NIRB (see Figure 3), and stellar emission is the dominant component, we neglect here the nebular emission.

In this case L_ν is just a blackbody spectrum, and we truncate it at $h\nu = 13.6$ eV, as done in Fernandez & Komatsu (2006); Fernandez et al. (2010); Cooray et al. (2012).

We plot the emissivity at $z = 10$ calculated by different methods in Figure 8 for a star formation efficiency $f_\star = 0.01$ and a minimum mass $M_{\min} = 10^6 M_\odot$. It is not surprising that “Approximation 2” overestimates the emissivity, since it assumes no stars die. However, we find that for the stellar mass range $1 - 100 M_\odot$, “Approximation 1” also overestimates the emissivity when $h\nu < 8$ eV. This happens because of the contribution of low mass stars whose lifetime is even longer than the age of the universe at that redshift, so that $\tau(m) < t_{\text{SF}}$ is not fulfilled. However, high energy photons come mainly from massive stars, which satisfy $\tau(m) < t_{\text{SF}}$. So at high energies, “Approximation 1” results agree well with the full analytical solution. The “Hybrid” approximation however, is more accurate through the entire energy range shown in Figure 8; yet, the results still deviate from the full analytical solution.

Still, the emissivity calculated from the template of Starburst99 is higher than the results obtained from the full analytical solution of Eqs. (A1-A4) with fitting formulae. This is mainly due to the full stellar evolutionary tracks used by Starburst99, which extend beyond the zero-age main sequence (ZAMS) stage. For example, the luminosity of a $7 M_\odot$ star with metallicity $1/50 Z_\odot$ at the end of the main sequence is three times as large as the ZAMS luminosity; at the end of its evolution, the luminosity is $\sim 10\times$ higher compared to ZAMS luminosity. The analogous value for a $100 M_\odot$ star of the same metallicity, is about $2\times$ the ZAMS luminosity.

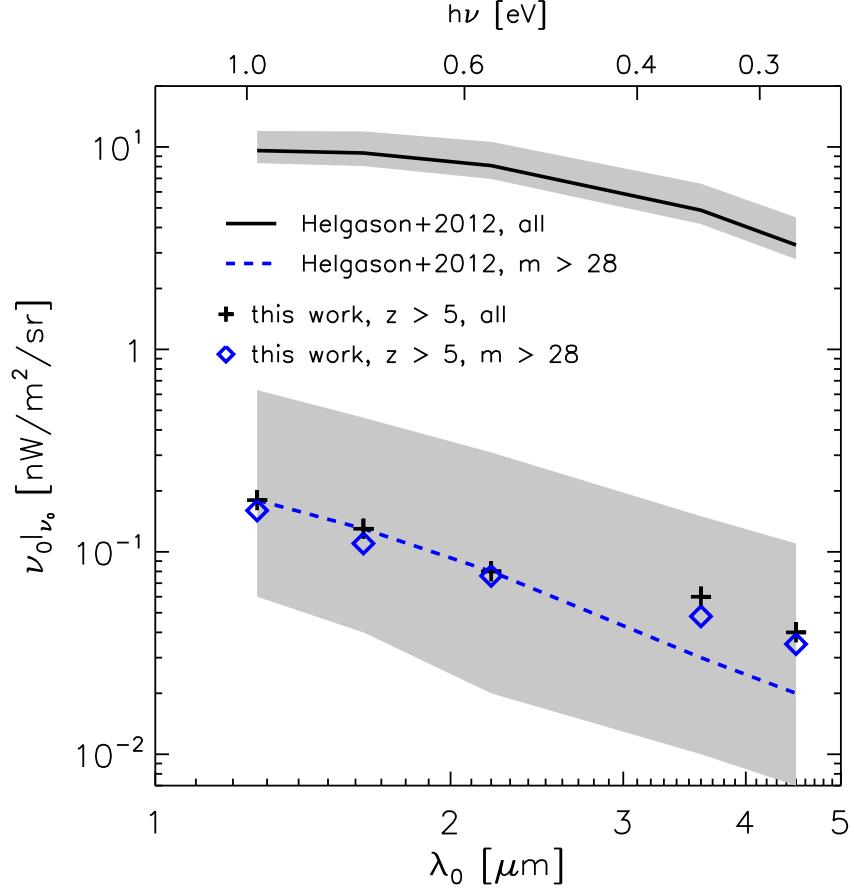


Fig. 4.— NIRB flux in the $1.25 \mu\text{m}$ to $4.5 \mu\text{m}$ wavelength range. The solid line is the flux from all galaxies from the default model in Helgason et al. (2012), while the dashed line is the remaining flux after removal of all sources brighter than $m_{\text{lim}} = 28$. The grey regions refer to the flux range between the maximum and minimum evolution scenarios in Helgason et al. (2012). As a comparison, we plot the flux from all galaxies with $z > 5$ in our work (crosses), and the flux after removal of sources down to $m_{\text{lim}} = 28$ (diamonds). Before any galaxy removal, the flux from galaxies with $z > 5$ is only a few percent of the overall flux in Helgason et al. (2012), i.e. the low- z galaxies dominate. However, after removal of galaxies with $m_{\text{lim}} < 28$, the flux from the remaining galaxies at all redshifts in Helgason et al. (2012) is comparable with that from the remaining galaxies with $z > 5$ in our work.

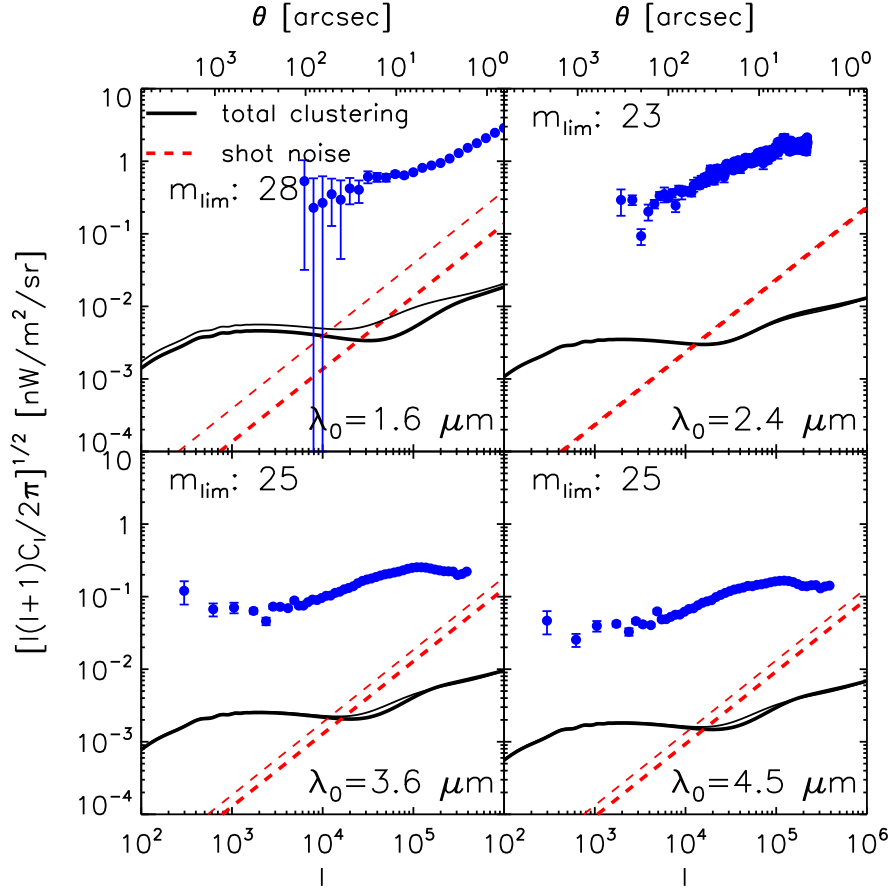


Fig. 5.— NIRB fluctuations angular power spectrum at different (observer frame) wavelengths, as labeled in each panel. The solid (dashed) lines refer to galaxy clustering (shot noise), the thick (thin) lines show the case with (without) removal of bright galaxies. We also plot the observations at wavelength $1.6 \mu\text{m}$ (Thompson et al. 2007a), $2.4 \mu\text{m}$ (Matsumoto et al. 2011), $3.6 \mu\text{m}$ and $4.5 \mu\text{m}$ (Kashlinsky et al. 2012, uncorrected for masking effects) by filled circles with errorbars.

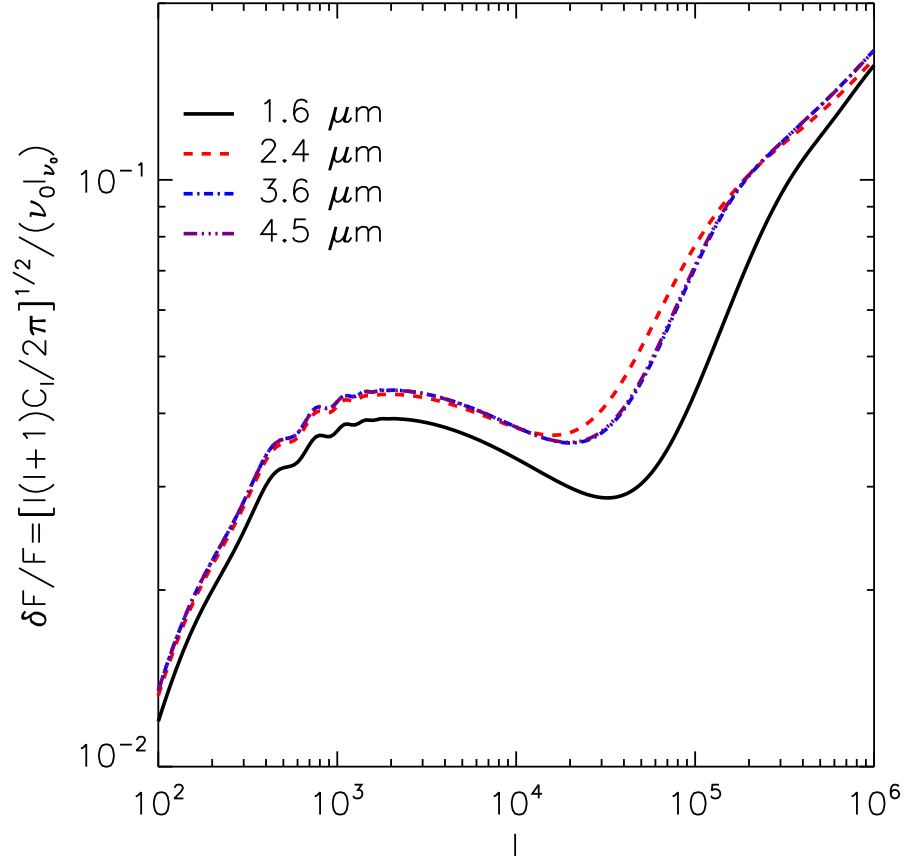


Fig. 6.— The ratio of $\delta F / F$ as a function of l for four different wavelength.

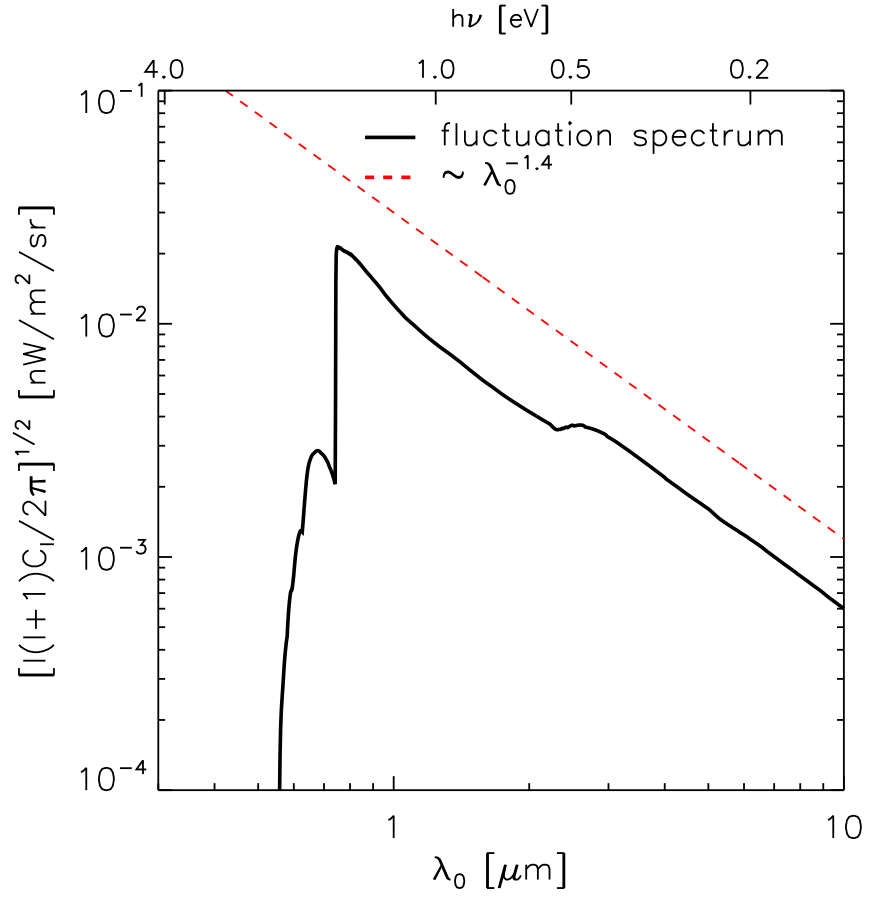


Fig. 7.— The spectrum of the NIRB fluctuations (solid line) at $l = 2000$, the dashed line shows a $\lambda_0^{-1.4}$ law.

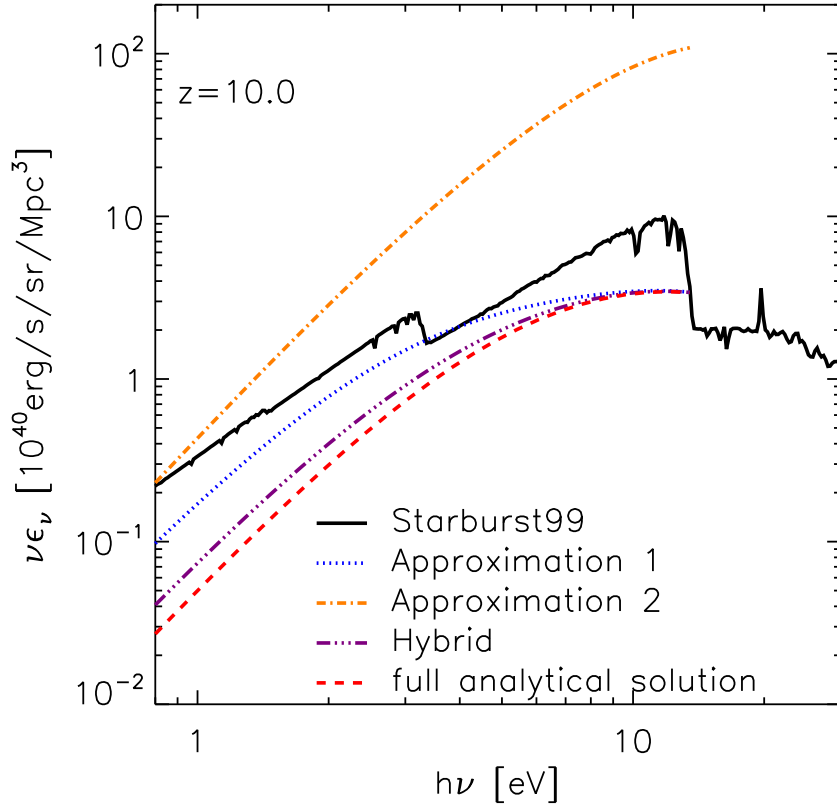


Fig. 8.— Emissivity of Pop II stars at redshift 10.0. The solid line is the result obtained by using the spectrum template from Starburst99 used here, the dotted line is for the “Approximation 1”; dash-dotted line refers to “Approximation 2”. The dash-dotted-dotted-dotted line corresponds to the “Hybrid” approximation; finally the dashed line refers to the full analytical solution of Eqs (A1-A4) using fitting formulae (see text).